FISEVIER

Contents lists available at ScienceDirect

Journal of Membrane Science

journal homepage: www.elsevier.com/locate/memsci



Supercritical ethane processing of ZIF-71 membrane towards superior H_2/SF_6 separation

Kunpeng Yu^a, Meng Ge^a, Mingming Wu^a, Taotao Ji^a, Lin Li^a, Jiahui Yan^a, Shengyan Meng^a, Chen Wang^a, Wenjing Hu^a, Wenwen Dong^a, Jianzhong Yin^{a,*}, Yi Liu^{a,b,**}

ARTICLE INFO

Keywords: Metal-organic framework ZIF-71 membrane Supercritical fluids Gas separation Ethane

ABSTRACT

Supercritical processing holds great promise for sustainable fabrication of high-performance MOF membranes; nonetheless, the generality and superiority of this protocol are still waiting to be explored. In this study, supercritical ethane (scC_2H_6) was used as the solvent for ZIF-71 membrane processing. Experimental results indicated that compared with common solvents, both nucleation and crystallization kinetics of ZIF-71 crystallites could be deliberately tailored in scC_2H_6 environments. Under optimized conditions, well-intergrown ZIF-71 membrane with H_2/SF_6 selectivity reaching 473.3 could be obtained through facile in situ growth; moreover, owing to effective elimination of grain boundary defects in the membrane, superior and stable H_2/SF_6 separation performance could be maintained at feed pressure up to 6 bar. Our research convincingly confirmed that SCF processing represented a facile and reliable protocol for preparing diverse MOF membranes with superior separation performances.

1. Introduction

In recent decades, metal-organic framework (MOF) has demonstrated great potential as competent membrane candidate due to the high separation efficiency [1–3], low energy cost, and small footprint [4–8]. Grain boundary defects, however, which may give rise to non-selective diffusion pathways for guest molecules, may negatively influence separation performances of MOF membranes under practical operation conditions [9–12]. Several protocols, such as microwave heating [13–16], interfacial microfluidic processing [17–19], and electrochemical synthesis [20–24], have been developed to reduce grain boundary defects in MOF membranes. Nonetheless, under most conditions, it remained impractical to maintain stable separation performance under varying operation conditions (e.g., at elevated pressure). Therefore, developing new protocols enabling effective elimination of grain boundary defects in MOF membranes has become indispensable [25, 56].

Supercritical fluid (SCF) [26-29], which possesses the density

comparable to liquids and diffusivity similar to gases with no surface tension [30,31], enables rapid diffusion of nutrients at the fluid-substrate interface, facilitating elimination of grain boundary defects in MOF membranes [32-34]; moreover, high sensitivity of physicochemical properties of SCF to operation conditions makes it possible for deliberate regulation of nucleation and reaction kinetics of MOF crystallites on the substrate. Recently we pioneered SCF processing of ZIF-8 membranes towards high-efficiency C₃H₆/C₃H₈ separation [35–39]. Among various SCFs, employing supercritical C₂H₆ (scC₂H₆) as reaction medium was found to be optimal for the formation of ZIF-8 membranes with fewer grain boundary defects due to its intrinsic chemical inertness and lower viscosity under comparable conditions, resulting in pressure-resistant C₃H₆/C₃H₈ selectivity. It should be noted that although significant progress has been made in SCF processing of MOF membranes, the type of MOF membranes recognized suitable for SCF processing is limited to isostructural ZIF-8 structures [40] (e.g., ZIF-8 and ZIF-67). The generality of SCF processing for preparing MOF membranes with superior separations, however, is still waiting to be

E-mail addresses: jzyin@dlut.edu.cn (J. Yin), diligenliu@dlut.edu.cn (Y. Liu).

a State Key Laboratory of Fine Chemicals, Frontiers Science Center for Smart Materials, School of Chemical Engineering, Dalian University of Technology, Dalian, 116024. China

b Dalian Key Laboratory of Membrane Materials and Membrane Processes, Dalian University of Technology, Dalian, 116024, China

^{*} Corresponding author.

^{**} Corresponding author. State Key Laboratory of Fine Chemicals, Frontiers Science Center for Smart Materials, School of Chemical Engineering, Dalian University of Technology, Dalian, 116024, China.

explored.

ZIF-71, a zeolitic imidazolate framework material with RHO topology consisting of zinc ions coordinated with 4,5-dichloroimidazole (dcIm) ligands [41–45], comprises a 8 MR nominal 4.8 Å pore size [46–48], rendering it a superb candidate for precise discrimination of gas mixtures with kinetic diameters in this range (e.g., $\rm H_2/SF_6$ separation). For instance, with DMF as solvent, Lin et al. [49] fabricated ZIF-71 membrane with He/SF₆ selectivity of 141.7 and He permeance of 2.37 \times 10^{-7} mol m $^{-2}$ s $^{-1}$ Pa $^{-1}$. Jin et al. [50] developed a contra-diffusion protocol to prepare hollow fiber-supported ZIF-71 membrane with ethanol/water separation factor (SF) of 6.9 and permeate flux of 2.6 kg/m 2 h at 25 °C. Nonetheless, owing to uncontrolled nucleation and growth kinetics of ZIF-71 crystals in common organic solvents, it remained difficult to eliminate grain boundary defects in the membrane, resulting in severe decay in selectivity upon being subjected to elevated-pressure operation.

Targeting at pressure-resistant H2/SF6 separation, in this study, we pioneered the preparation of ZIF-71 membrane through SCF processing (Fig. 1). scC₂H₆ was selected as reaction medium, considering its wide supercritical region, pH neutrality, and chemical inertness, which was beneficial for retarding bulk nucleation in bulk solution and promoting intergrowth between adjacent ZIF-71 crystallites on substrate surface. In addition, sol-gel-derived ZnO buffer layer, which was partially embedded in substrate pores, not only served as zinc source of ZIF-71 layer but also resulted in the formation of semi-confined membrane structure, which was beneficial for maintaining membrane structure integrity even at elevated operation pressure. Gas permeation results implied that our membrane achieved H₂/SF₆ SF as high as 426.5 under ambient conditions; of particular note, its SF further increased to 478.2 upon elevating feed pressure to 6 bar, validating the competency of scC₂H₆ processing in eliminating grain boundary defects in the membrane.

2. Experimental section

2.1. Materials

Zinc nitrate hexahydrate ($H_{12}N_2O_{12}Zn$, 99.0 %, Sinopharm), 4,5-Dichloroimidazole (dcIm, $C_3H_2Cl_2N_2$, 98.0 %, Macklin), 2-methylimidazole (2-mIm, $C_4H_6N_2$, 99.0 %, Macklin), 2-methoxyethanol ($C_3H_8O_2$, 99.0 %, Aladdi), zinc acetate ($C_4H_6O_4Zn$, 99.0 %, Macklin),

hydrochloric acid (HCl, 36.0–38.0 wt% in $\rm H_2O$, Sinopharm), ethanolamine ($\rm C_2H_7NO$, 99.0 %, Aladdi), methanol ($\rm CH_4O$, 99.5 %, Kemiou), ethanol ($\rm C_2H_6O$, 99.7 %, Kemiou), deionized water (home-made). Experimental and test gases including $\rm H_2$, $\rm SF_6$ and $\rm Ar$ (99.999 %, Dalian Junfeng Gas Chemical Co., Ltd). No further purification is required before use.

2.2. Deposition of ZnO buffer layers

The preparation of a uniform ZnO layer follows previously reported methods: to prevent excessive penetration of the Zn-based gel and enhance the uniformity of the gel on the substrate surface, a layer of 0.2 wt% ZIF-8 crystal suspension with particle size of $\sim\!70$ nm was spin-coated onto the $\alpha\text{-Al}_2O_3$ substrate surface (3000 rpm, 60 s, 0.2 ml). After drying at 70 °C for 30 min, Zn-based gel was spin-coated onto the surface at the same speed and dried at 70 °C for 30 min. Subsequently, the substrate plates were placed in a muffle furnace and calcined at 450 °C for 2 h to obtain a pure-phase ZnO buffer layer supported by $\alpha\text{-Al}_2O_3$ substrate. The heating and cooling rates were both 1 °C/min, and the gel spin-coating process was repeated twice.

2.3. Supercritical ethane experimental process

To ensure the uniformity of the reaction and avoid ligand loss during pressurization for recovery and reuse, laboratory-made microporous reaction inserts were used to fix the substrate plates and ligands, which were then placed in a high-pressure reactor (Fig. S1). The reactor was evacuated to remove internal air before the valve of gas cylinder was opened, and the reactor and pipe line were repeatedly purged with ethane to replace any residual gases, ensuring that the internal reaction medium was pure ethane. After the replacement was complete, the reactor was preheated to ensure that the temperature inside the reactor was above the critical temperature of ethane before pressurization. Subsequently, a pneumatic pressure pump was used to pressurize the reactor to the preset pressure, and reaction was allowed to proceed for 24 h. After reaction, the internal pressure was slowly released when the heating jacket turned off, and unreacted 4,5-dichloroimidazole ligand was recovered.

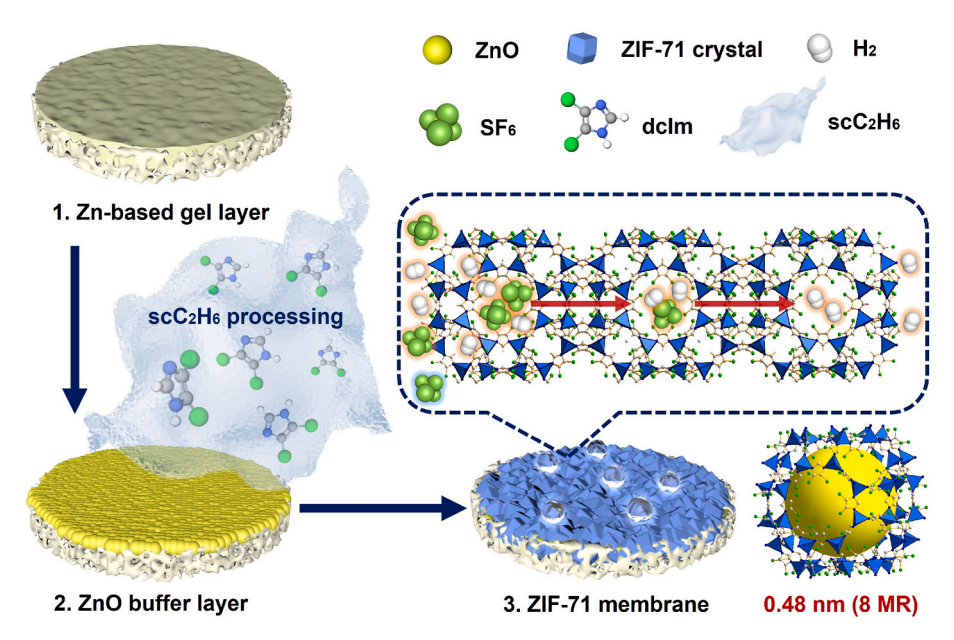


Fig. 1. Schematic illustration of scC₂H₆ processing of ZIF-71 membranes.

3. Results and discussion

3.1. Synthesis of ZIF-71 membrane on porous α -Al₂O₃ substrate using scC₂H₆ as the solvent

The first step involved the introduction of ZnO buffer layer on porous α-Al₂O₃ substrate (Fig. 2a–S2 and S3). As shown in Fig. 2b, after spincoating deposition and calcination of Zn-based gel, the substrate surface had been uniformly covered with smooth ZnO buffer layer with a thickness \sim 2 µm (Fig. S2h and S4). Cross-sectional SEM image further revealed that obtained ZnO buffer layer remained partially penetrated into substrate pores with penetration depth much thinner than the buffer layer prepared in the absence of ZIF-8 crystal layer (Fig. S4). A closer look at the sample surface implied that the ZnO buffer layer was composed of 30 nm-sized primary particles, which were further agglomerated into 200 nm-sized secondary particles (Fig. S2g and S2h). Considering high reactivity of ZnO primary particles due to high surface free energy and dangling bond density as well as the semi-confined structure which was beneficial for maintaining strong adhesion of the ZIF-71 layer on the substrate, the Zn-based gel-derived ZnO buffer layer was selected as metal source of ZIF-71 membrane during scC₂H₆ processing.

Subsequently, the ZnO buffer layer was immersed in a supercritical reactor containing an excess amount of dcIm ligand powders. Based on reaction parameters, obtained ZIF-71 membranes were defined as ZIF-71m_{P-T(IG)}, where *P* denoted reaction pressure, *T* denoted reaction temperature, and IG indicated in situ growth. As illustrated in Fig. 2 and S5, a clear transition of the membrane surface from amorphous state to ZIF-71 phase was observed with increasing temperature and pressure in the range of 60–90 °C and 6–10 MPa [51]. To be specific, at 6 MPa and 60 °C, ZIF-71m_{6-60(IG)} exhibited a smooth surface morphology with clearly visible interface between the formed layer and the substrate accompanying with partial penetration into substrate pores (Fig. 2c and d and S6), while the absence of diffraction peaks derived from ZIF-71

phase (Fig. 2j) implied that this reaction condition was not sufficient to trigger ZIF-71 nucleation on the substrate [52,53].

Under optimized reaction conditions of 6 MPa and 90 °C, ZIF-71m₆-90(IG) with a thickness of ~1.2 µm was readily obtained (Fig. 2e and f). The SEM image indicated that its grain size reached ~800 nm with no visible grain boundary defects. Corresponding EDXS spectra (Fig. 2g) clearly indicated the penetration of both ZnO buffer layer and ZIF-71 layer. Obviously, elevating reaction temperature facilitated heterogenous nucleation and growth of ZIF-71 crystallites on the substrate surface, which was crucial for promoting intergrowth between adjacent ZIF-71 crystallites. XRD pattern further confirmed that the formed layer belonged to pure ZIF-71 phase (Fig. 2j). Fourier transform infrared (FT-IR) spectrum (Fig. 2k) showed absorption peaks at 600-800 cm⁻¹, corresponding to C–Cl stretching vibrations and a characteristic peak at 1053 cm⁻¹ assignable to in-plane ring deformation of the imidazole and C-N stretching vibrations; while absorption peaks at 1201 cm⁻¹, 1234 cm⁻¹, and 1301 cm⁻¹ (associated with C-N stretching vibrations), which were coincident with the results reported in the literature [45,

We further investigated the influence of reaction pressure on membrane morphology. Experimental results revealed that under reaction condition of 10 MPa and 90 °C, a top wrinkled layer appeared on the surface of ZIF-71m_{10-90(IG)}. After repeated washing with methanol, the wrinkled layer was partially detached, resulting in exposure of larger grain-sized (>5 μ m) ZIF-71 membrane underneath (Fig. 2h and i and S5). This could be attributed to coupled effects of enhanced reagent reactivity and increased ligand solubility, resulting in excessive bulk nucleation and crystallization of ZIF-71 crystallites. Obviously, overconsumption of nutrients in the bulk solution resulted in insufficient driving force for complete elimination of grain boundary defects in the membrane [55]. Considering the degree of intergrown of ZIF-71 membranes, the optimal scC₂H₆ reaction condition was fixed at 6 MPa and 90 °C for 24 h.

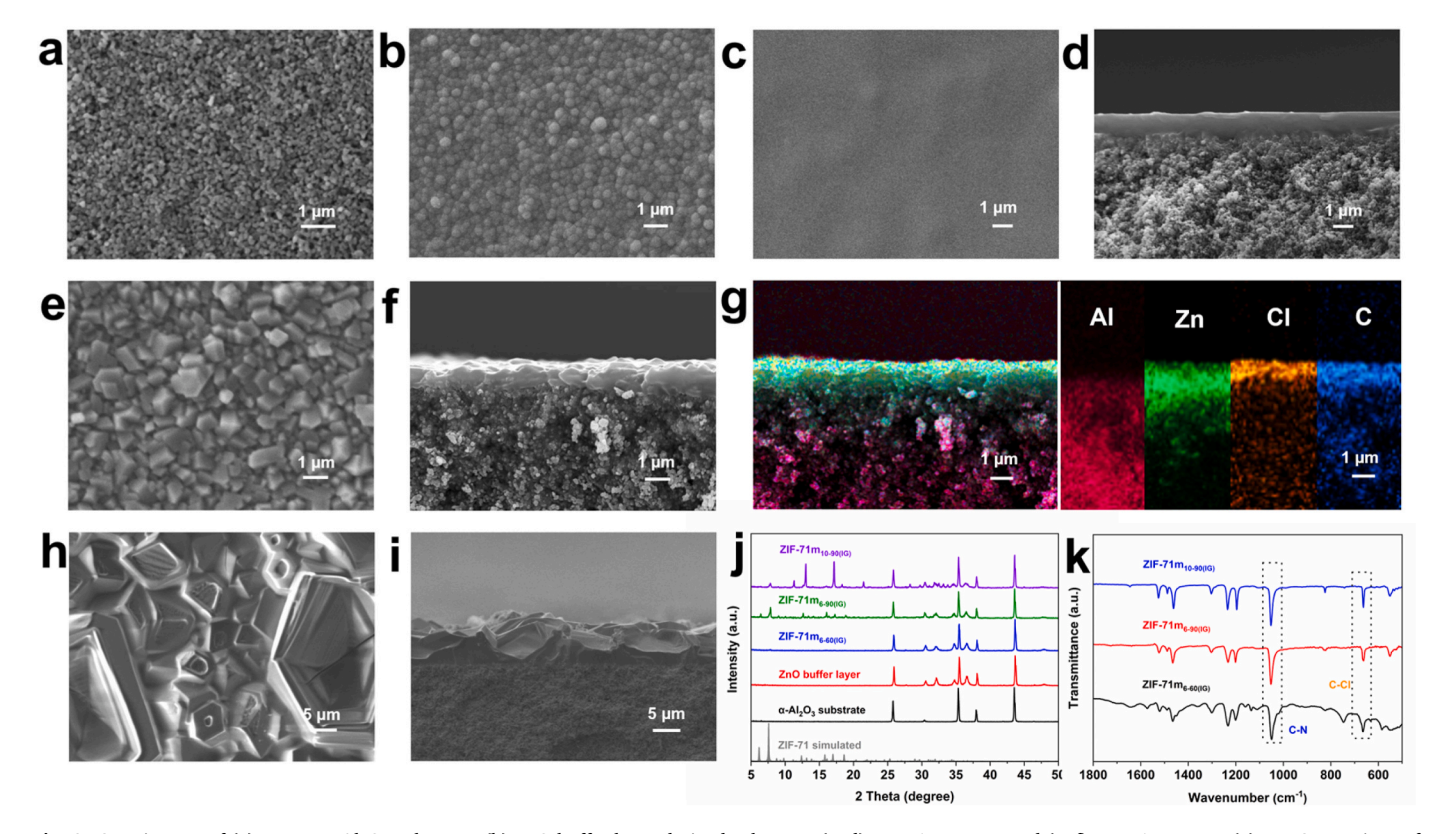


Fig. 2. SEM images of (a) porous α -Al₂O₃ substrate, (b) ZnO buffer layer-derived substrate, (c, d) ZIF-71m_{6-60(IG)}, and (e, f) ZIF-71m_{6-90(IG)}. (g) EDXS mappings of ZIF-71m_{6-90(IG)}. (h, i) SEM images of ZIF-71m_{10-90(IG)}. (j) XRD patterns and (k) FT-IR spectra of ZIF-71 membranes prepared under varying reaction conditions.

3.2. Microscopic structure and intergrowth quality characterization of scC₂H₆-synthesized ZIF-71 membranes

To finely investigate the grain boundary structure, STEM characterization was carried out on ZIF-71m_{6-90(IG)}. HAADF-STEM images (Fig. 3a and S7) revealed that the ZIF-71 layer was readily embedded into the substrate pores; moreover, line distribution plots of corresponding elements showed penetration depth of the ZIF-71 layer was higher than 500 nm (Fig. 3b and c). Simultaneously, no obvious grain boundary defects could be discerned in HRTEM images (Fig. 3d and e), confirming a defect-free nature of ZIF-71m_{6-90(IG)}. As shown Fig. 4d, the presence of fewer grain boundary defects in ZIF-71m_{6-90(IG)} could be further convinced with lower R_a value of 32.6 nm (Fig. 4a–c) compared with that of ZnO buffer layer ($R_a = 40.2$ nm).

We further magnified the penetration zone in Fig. 3d and e. As shown in Fig. 3f and g, HRTEM results showed not only relatively clear diffraction spots belonging to (110) plane of ZnO and (110) plane of Al $_2$ O $_3$, but also diffraction spots near the center. This faint diffraction arc, with relatively lower intensity compared with the ZnO ring, was consistent with the low-angle diffraction (332) characteristics and large lattice fringe distance of ZIF-71 (Fig. 3l). Owing to different observation angles, lattice fringes corresponding to (320) and (220) planes of ZIF-71 could also be observed in different areas of membrane penetration zone (Fig. 3h–k).

Unfortunately, ZIF-71 crystal structure cannot survive under highenergy electron beams, making it difficult to directly observe the diffraction peak fringes belonging to ZIF-71. For comparison, by referring to previous literature [57], \sim 500 nm-sized ZIF-71 nanoparticles with high crystallinity were synthesized by solvothermal method (Fig. S8a and S8b) and characterized by HRTEM under the same conditions. As shown in Fig. S8c—e, even though ZIF-71 crystals exhibited ideal crystal morphology and high crystallinity, the lattice fringes of ZIF-71 still could not be clearly discerned. The missing diffraction intensity may be attributed to partial amorphization or crystal degradation caused by high-energy electron beam during HRTEM imaging [58–62].

Nevertheless, we were still able to observe lattice fringes belonging to three phases in the deeper penetration zone by taking advantage of the protective effect of electron beam stable phase (i.e., ZnO and $\alpha\text{-Al}_2O_3$). This result confirmed that ZnO and ZIF-71 had successfully generated into $\alpha\text{-Al}_2O_3$ substrate pores, forming a three-phase coupling zone, which played a critical role in enhancing structural integrity and mechanical strength of the membrane.

For comparation, in parallel we prepared ZIF-71 membranes through solvothermal method and $\rm scCO_2$ processing. Upon using DMF as solvent, the ZnO buffer layer tended to peel off from the substrate surface, resulting in the generation of large areas of open space on the substrate surface after solvothermal growth (Fig. S9a–f and S10a-c). While with methanol as solvent, the nucleation rate of ZIF-71 remained too low even upon increasing the reaction temperature to 60 °C (Fig. S9g and S9h), resulting in the difficulty in obtaining well-intergrown ZIF-71 membrane.

Alternatively, we tried growing ZIF-71 membrane with $scCO_2$ as solvent within a temperature and pressure range similar to that of scC_2H_6 (Fig. S9i–p and S10e-h). Experimental results indicated that within the upper limit of reactor temperature of 110 °C, the substrate

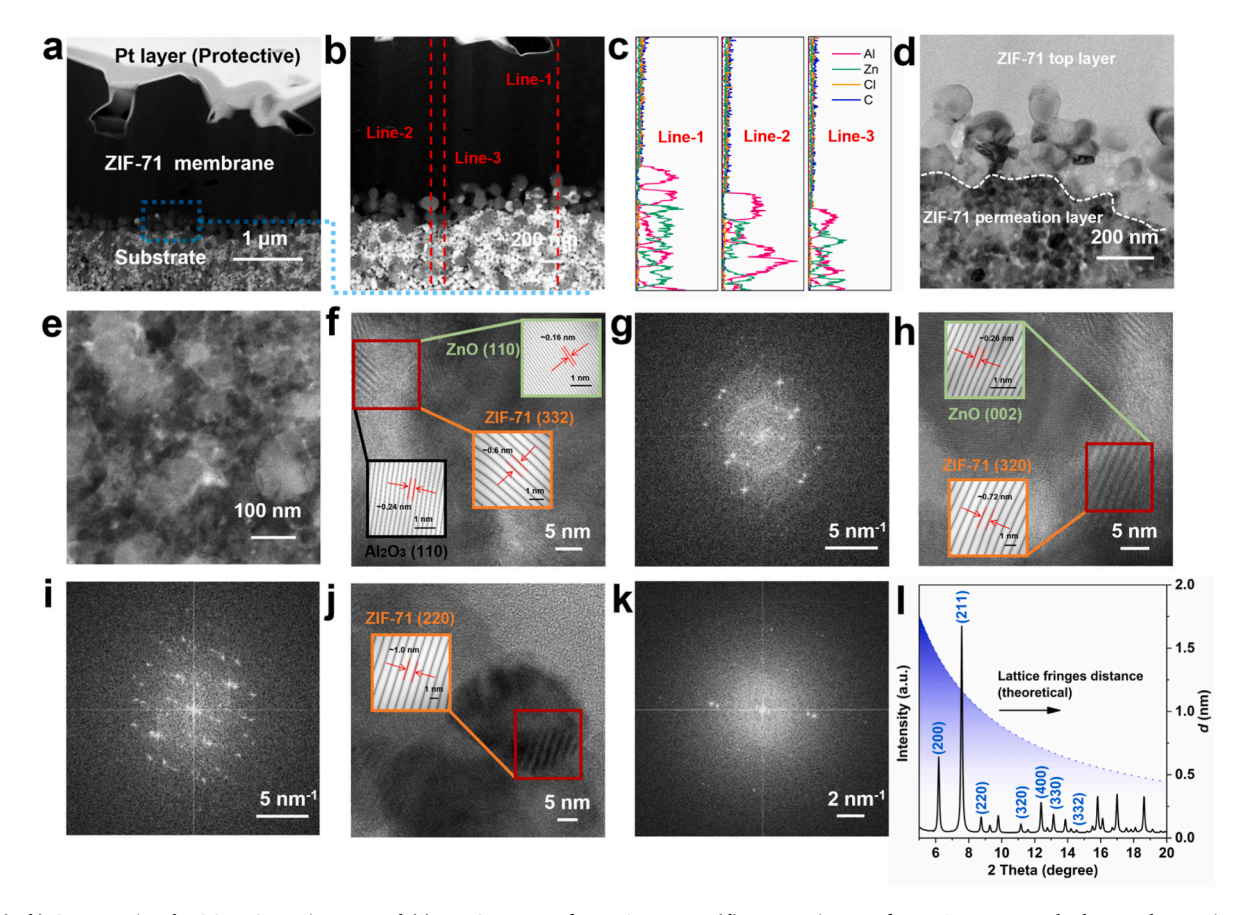


Fig. 3. (a, b) Cross-sectional HAADF-STEM images and (c) EDXS spectra of ZIF-71 $m_{6.90(IG)}$. (d) HRTEM image of ZIF-71 $m_{6.90(IG)}$ at the layer-substrate interface. (e) HRTEM image of ZnO-enriched permeation area and corresponding local high-resolution images: (f) ZIF-71/ZnO/ α -Al $_2$ O $_3$ coupling zone and (g) corresponding FFT pattern, (h) ZIF-71/ZnO coupling zone and (i) corresponding FFT pattern, and (j) ZIF-71-enriched zone and (k) corresponding FFT pattern. (l) The simulated XRD pattern of ZIF-71.

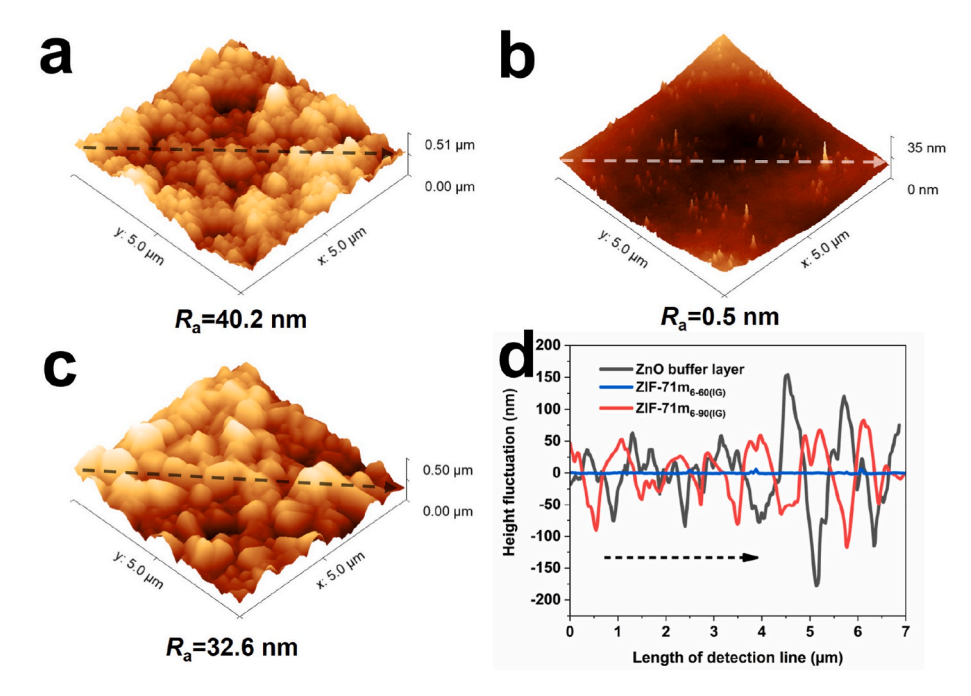


Fig. 4. AFM image and surface roughness of (a) ZnO buffer layer, (b) ZIF-71 $m_{6-60(IG)}$, and (c) ZIF-71 $m_{6-90(IG)}$. (d) Surface height fluctuation curves of ZnO buffer layer, ZIF-71 $m_{6-60(IG)}$, and ZIF-71 $m_{6-90(IG)}$.

surface remained mainly composed of unreacted ZnO buffer layer with sparse ZIF-71 crystallites covered on its surface. Therefore, scC_2H_6 solvent was more suitable for obtaining well-intergrown ZIF-71 membranes with few grain boundary defects.

3.3. Gas separation performance of scC_2H_6 -synthesized ZIF-71 membrane

Finally, gas permeation properties of ZIF-71 $m_{6.90(IG)}$ were measured in Wicke-Kallenbach gas permeation apparatus (Fig. S11). We first investigated single gas permeation behavior of ZIF-71 $m_{6.90(IG)}$. As shown in Fig. 5a, the permeance of gas molecules steadily decreased with increasing kinetic diameters. As shown in Fig. 5a, H₂ molecules

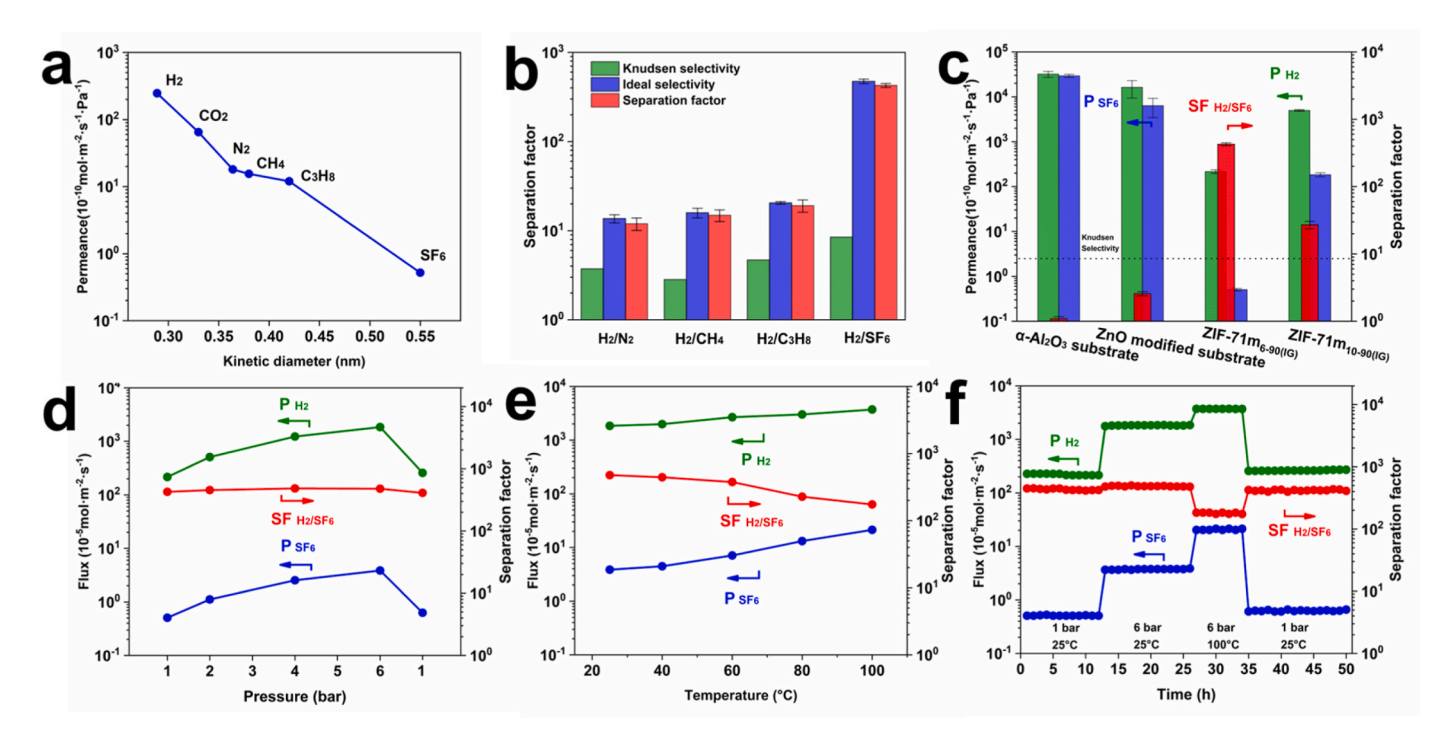


Fig. 5. (a) Single gas permeance and (b) ideal selectivity of different gas pairs through ZIF-71 $m_{6-90(IG)}$. (c) H_2/SF_6 separation performances of ZIF-71 membranes prepared under different reaction conditions. (d) The effect of feed pressure on H_2/SF_6 separation performance of ZIF-71 $m_{6-90(IG)}$ at operation temperature of 25 °C. (e) The effect of operation temperature on H_2/SF_6 separation performance of ZIF-71 $m_{6-90(IG)}$ at feed pressure of 6 bar. (f) Long-term stability of ZIF-71 $m_{6-90(IG)}$ under varying operation conditions.

exhibited the highest permeance of 2.5×10^{-8} mol m^{-2} s $^{-1}$ Pa $^{-1}$ with ideal selectivity of $H_2/N_2,\ H_2/CH_4,\ H_2/C_3H_8$ and H_2/SF_6 gas pairs reaching 13.8, 15.9, 20.5 and 473.3, respectively (Fig. 5b), which was remarkably higher than their Knudsen selectivity. Aiming at practical applications, the H_2/SF_6 separation performance of ZIF-71m_{6-90(IG)} was further studied at varying operation pressures. As shown in Fig. 5c, SF of equimolar H_2/SF_6 mixture reached 426.5 with H_2 permeance of 2.2 \times 10^{-8} mol m $^{-2}$ s $^{-1}$ Pa $^{-1}$ at feed pressure of 1 bar. In contrast, owing to the existence of grain boundary defects in ZIF-71m_{10-90(IG)}, its H_2 permeance reached higher than 5.0×10^{-7} mol m $^{-2}$ s $^{-1}$ Pa $^{-1}$ at the expense of inferior H_2/SF_6 SF of 27.1; while ZIF-71m_{6-60(IG)} exhibited H_2 permeance was lower than 1.0×10^{-10} mol m $^{-2}$ s $^{-1}$ Pa $^{-1}$, possibly owing to the blockage of ZIF-71 pores by the amorphous layer.

Aiming at practical applications, the influence of operation conditions on $\rm H_2/SF_6$ separation performance of ZIF-71m_6-90(IG) was further investigated. Upon elevating operation pressure from 1 to 6 bar, both $\rm H_2/SF_6$ SF and $\rm H_2$ permeance of ZIF-71m_6-90(IG) steadily increased to 478.2 and $\rm 3.1\times10^{-8}~mol~m^{-2}~s^{-1}~Pa^{-1}$ (Fig. 5d), which was indicative of the presence of few grain boundary defects in the membrane. Furthermore, the effect of operation temperature on $\rm H_2/SF_6$ separation performance of ZIF-71m_6-90(IG) at operation pressure of 6 bar was studied. It was found that increasing operation temperature led to concurrent increase of $\rm H_2$ and SF_6 permeance (Fig. 5e). In comparison, the increase of SF_6 permeance was more pronounced than that of $\rm H_2$, causing gradual reduction in $\rm H_2/SF_6$ SF from 478.2 to 174.5 upon increasing temperature from 25 to 100 °C. This could be attributed to enhanced flexibility of ZIF-71 framework with increasing operation temperature.

We finally investigated the operation stability of ZIF-71 $m_{6.90(IG)}$. As shown in Fig. 5f, our membrane maintained superior and steady H_2 permeance and H_2/SF_6 SF at pressures varying from 1 to 6 bar and temperatures varying from 25 to 100 °C during continuous operation for 50 h, which was conducive to their practical applications under harsh conditions. Simultaneously, long-term operation stability (Fig. S12) and reproducibility (Table S1) of ZIF-71 membranes were verified. As shown in Fig. S12, ZIF-71 membrane obtained under optimized conditions exhibited stable H_2/SF_6 separation performance within 5 days, which was indicative of long-term operation stability.

To verify the chemical stability and reusability of ligands in scC_2H_6 reaction system, the morphology and structure of the recovered ligand samples after multiple repeated reactions were analyzed and compared with the original ligands. Fig. S13a and S13b represented SEM images of the original and secondly recovered dcIm ligands, respectively. Obviously, no significant physical degradation or morphological damage of dcIm ligands occurred during the reaction process.

The functional integrity of the original ligands, firstly recovered ligands, and secondly recovered ligands were further analyzed by FT-IR spectroscopy (Fig. S13c). Our results showed that all three samples exhibited consistent absorption peaks within the range of 600–1800 cm $^{-1}$ including the C–N stretching vibrations ($\sim\!1053~{\rm cm}^{-1}$) and C–Cl stretching vibrations ($\sim\!750~{\rm cm}^{-1}$), and there was no significant discrepancy in the position and intensity of these absorption peaks, indicating that chemical structure of recovered ligands remained unchanged. Furthermore, the XRD pattern (Fig. S13d) confirmed that the crystal structure of the ligands did not change before and after recovery. All three samples showed consistent diffraction peak positions and intensity distributions, matching the standard diffraction patterns of dcIm ligands. Above results indicated that dcIm ligands were not degraded during scC₂H₆ processing.

4. Conclusions

In this study, we pioneered the preparation of ZIF-71 membranes with controlled microstructure through scC_2H_6 processing. Owing to intrinsic chemical inertness and lower viscosity of $scCO_2$ under comparable conditions, grain boundary defects in the membrane could be

effectively sealed, resulting in pressure-resistant performance. Gas permeation results indicated that ZIF-71 membrane prepared under optimized conditions exhibited H₂/SF₆ SF of 426.5 under ambient conditions, while further increasing operation pressure to 6 bar led to increased H₂/SF₆ SF of 478.2. Through combining with excellent long-term operation stability, our membrane held great promise for sustainable preparation of diverse MOF membranes with optimized microstructure and superior separation performances.

CRediT authorship contribution statement

Kunpeng Yu: Writing – original draft, Methodology, Investigation, Formal analysis, Data curation, Conceptualization. Meng Ge: Conceptualization, Supervision. Mingming Wu: Methodology, Data curation. Taotao Ji: Investigation, Formal analysis. Lin Li: Investigation. Jiahui Yan: Supervision. Shengyan Meng: Investigation. Chen Wang: Supervision. Wenjing Hu: Investigation. Wenwen Dong: Supervision. Jianzhong Yin: Supervision, Methodology, Conceptualization. Yi Liu: Writing – review & editing, Supervision, Resources, Methodology, Funding acquisition, Conceptualization.

Declaration of competing interest

The authors declare that they have no known competing financial interests or personal relationships that could have appeared to influence the work reported in this paper.

Acknowledgements

The authors are grateful to the National Natural Science Foundation of China (22478056, 22408038), Postdoctoral Fellowship Program of CPSF GZC20230355, Science Fund for Creative Research Groups of the National Natural Science Foundation of China (22021005), National Key Research and Development Program of China (2023YFB3810700), Liaoning Province Funds for Distinguished Young Scholars (2024JH3/50100002), Liaoning Binhai Laboratory (LBLG-2024-07), State Key Laboratory of Catalysis (2024SKL-A-003), and Science and Technology Innovation Fund of Dalian (2024JJ12GX027) for the financial support.

Appendix A. Supplementary data

Supplementary data to this article can be found online at https://doi.org/10.1016/j.memsci.2025.124835.

Data availability

Data will be made available on request.

References

- D.S. Sholl, R.P. Lively, Seven chemical separations to change the world, Nature 532 (2016) 435–437.
- [2] M.R.A. Hamid, Y. Qian, R. Wei, Z. Li, Y. Pan, Z. Lai, H. Jeong, Polycrystalline metal-organic framework (MOF) membranes for molecular separations: engineering prospects and challenges, J. Membr. Sci. 640 (2021) 119802.
- [3] D. Lee, S. Lee, I. Choi, M. Kim, Positional functionalizations of metal-organic frameworks through invasive ligand exchange and additory MOF-on-MOF strategies: a review. Smart Mol 2 (2024) e20240002.
- [4] Y. Zhang, B.H. Yin, L. Huang, L. Ding, S. Lei, S.G. Telfer, J. Caro, H. Wang, MOF membranes for gas separations, Prog. Mater. Sci. 151 (2025) 101432.
- [5] D. Shi, X. Yu, W. Fan, V. Wee, D. Zhao, Polycrystalline zeolite and metal-organic framework membranes for molecular separations, Coord. Chem. Rev. 437 (2021) 213704
- [6] X. Li, Y. Liu, J. Wang, J. Gascon, J. Li, B. Van der Bruggen, Metal-organic frameworks based membranes for liquid separation, Chem. Soc. Rev. 46 (2017) 7124–7144.
- [7] W. Li, Metal-organic framework membranes: production, modification, and applications, Prog. Mater. Sci. 100 (2019) 21–63.
- [8] T. Ji, L. Liu, Y. Sun, Y. Liu, G. Xu, J. Yan, G. He, Y. Liu, Sub-zero temperature synthesis of pressure resistant ZIF-8 membrane with superior C_3H_6/C_3H_8 separation performance, ACS Mater. Lett. 4 (2022) 1094–1100.

- [9] Q. Hou, S. Zhou, Y. Wei, J. Caro, H. Wang, Balancing the grain boundary structure and the framework flexibility through bimetallic metal-organic framework (MOF) membranes for gas separation, J. Am. Chem. Soc. 142 (2020) 9582–9586.
- [10] Y. Xu, Y. Xiao, W. Zhang, H. Lin, L. Shen, R. Li, Y. Jiao, B. Liao, Plant polyphenol intermediated metal-organic framework (MOF) membranes for efficient desalination, J. Membr. Sci. 618 (2021) 118726.
- [11] F. Wang, H. Sun, M. Shen, J. Li, N. Wang, H. Meng, Q. An, Hydrophobic ultrathin MOF membranes with tuning pore structure for efficient alcohol-permselective pervaporation, J. Membr. Sci. 698 (2024) 122615.
- [12] T. Xia, Y. Wu, T. Ji, W. Hu, K. Yu, X. He, B.H. Yin, Y. Liu, Mixed-matrix membranes incorporating hierarchical ZIF-8 towards enhanced CO₂/N₂ separation, Smart Mol 3 (2025) e20240066.
- [13] M. Zhai, F. Moghadam, T. Gosiamemang, J.Y.Y. Heng, K. Li, Facile orientation control of MOF-303 hollow fiber membranes by a dual-source seeding method, Nat. Commun. 15 (2024) 10264.
- [14] A. Kasik, J. James, Y.S. Lin, Synthesis of ZIF-68 membrane on a ZnO modified α-Alumina support by a modified reactive seeding method, Ind. Eng. Chem. Res. 55 (2016) 2831–2839.
- [15] N. Rangnekar, N. Mittal, B. Elyassi, J. Caro, M. Tsapatsis, Zeolite membranes a review and comparison with MOFs, Chem. Soc. Rev. 44 (2015) 7128–7154.
- [16] Y. Sun, Y. Liu, J. Caro, X. Guo, C. Song, Y. Liu, In-Plane epitaxial growth of highly c-Oriented NH₂-MIL-125(Ti) membranes with superior H₂/CO₂ selectivity, Angew. Chem. Int. Ed. 57 (2018) 16088–16093.
- [17] A.J. Brown, N.A. Brunelli, K. Eum, F. Rashidi, J.R. Johnson, W.J. Koros, C. W. Jones, S. Nair, Interfacial microfluidic processing of metal-organic framework hollow fiber membranes, Science 345 (2014) 72–75.
- [18] K. Eum, A. Rownaghi, D. Choi, R.R. Bhave, C.W. Jones, S. Nair, Fluidic processing of high-performance ZIF-8 membranes on polymeric hollow fibers: mechanistic insights and microstructure control, Adv. Funct. Mater. 26 (2016) 5011–5018.
- [19] K. Eum, C. Ma, A. Rownaghi, C.W. Jones, S. Nair, ZIF-8 membranes via interfacial microfluidic processing in polymeric hollow fibers: efficient propylene separation at elevated pressures, ACS Appl. Mater. Interfaces 8 (2016) 25337–25342.
- [20] C. Jin, S. Liu, R. Zheng, Y. Li, X. Chen, J. Caro, J. Jiang, A. Huang, Electric field-driven assembly of (110) oriented metal-organic framework ZIF-8 monolayer with high hydrogen selectivity, Chem. Eng. J. 498 (2024) 155773.
- [21] X. Zhang, Y. Li, C. Van Goethem, K. Wan, W. Zhang, J. Luo, I.F.J. Vankelecom, J. Fransaer, Electrochemically assisted interfacial growth of MOF membranes, Matter 1 (2019) 1285–1292.
- [22] S. Nair, Electrons to membranes, Nat. Energy 6 (2021) 864-865.
- [23] S. Zhou, Y. Wei, L. Li, Y. Duan, Q. Hou, L. Zhang, L. Ding, J. Xue, H. Wang, J. Caro, Paralyzed membrane: current-driven synthesis of a metal-organic framework with sharpened propene/propane separation, Sci. Adv. 4 (2018) eaau1393.
- [24] F. Li, H. Zhang, F. Wu, X. Hou, Q. Xu, J. Li, Y. Guo, Z. Jiang, Magnetic-field-driven fabrication of robust metal-organic framework membranes for efficient Propylene/ Propane separation, Adv. Funct. Mater. 35 (2025) 2422400.
- [25] J. Wang, G. Li, Full-scale modeling of chemical experiments, Smart Mol. 2 (2024) e20230010.
- [26] U. Ranieri, F. Formisano, F.A. Gorelli, M. Santoro, M.M. Koza, A.D. Francesco, L. E. Bove, Crossover from gas-like to liquid-like molecular diffusion in a simple supercritical fluid, Nat. Commun. 15 (2024) 4142.
- [27] K. Nasrin, M. Arunkumar, N.K. Kumar, V. Sudharshan, S. Rajasekar, D. Mukhilan, M. Arshad, M. Sathish, A rationally designed hetero-assembly of 2D/2D Nitrogendoped MXene/Graphene via supercritical fluid processing for high energy durable supercapacitors, Chem. Eng. J. 474 (2023) 145505.
- [28] C.A. Eckert, B.L. Knutson, P.G. Debenedetti, Supercritical fluids as solvents for chemical and materials processing, Nature 383 (1996) 313–318.
- [29] V.E. Patil, J. Meeuwissen, L.J.P. van den Broeke, J.T.F. Keurentjes, Permeation of supercritical fluids across polymeric and inorganic membranes, J. Supercrit. Fluids 37 (2006) 367–374.
- [30] N.P. Longmire, S.L. Showalter, D.T. Banuti, Holding water in a sieve-stable droplets without surface tension, Nat. Commun. 14 (2023) 3983.
- [31] C.J. Clarke, W.C. Tu, O. Levers, A. Brohl, J.P. Hallett, Green and sustainable solvents in chemical processes, Chem. Rev. 118 (2018) 747–800.
- [32] Y. Xu, V. Musumeci, C. Aymonier, Chemistry in supercritical fluids for the synthesis of metal nanomaterials, React. Chem. Eng. 4 (2019) 2030–2054.
- [33] T. Adschiri, A. Yoko, Supercritical fluids for nanotechnology, J. Supercrit. Fluids 134 (2018) 167–175.
- [34] J.A. Darr, M. Poliakoff, New directions in inorganic and metal-organic coordination chemistry in supercritical fluids, Chem. Rev. 99 (1999) 495–541.
- [35] L. Liu, Y. Song, T. Ji, Y. Sun, D. He, H. Hu, Y. Liu, Beyond solution-based protocols: MOF membrane synthesis in supercritical environments for an elegant sustainability performance balance, ACS Mater. Lett. 2 (2020) 1142–1147.
- [36] L. Liu, T. Ji, W. Hu, Y. Sun, Y. He, J. Yan, G. He, Y. Liu, Epitaxial supercritical fluid processing of ZIF-8 membranes towards efficient C₃H₆/C₃H₈ separation, J. Membr. Sci. 669 (2023) 121300.
- [37] W. Hu, L. Liu, J. Yan, Y. Gao, T. Ji, K. Yu, S. Meng, M. Wu, X. Fan, W. Dong, Y. Liu, Sustainable fabrication of highly (110)-oriented ZIF-8 membrane via supercritical fluid processing, J. Membr. Sci. 707 (2024) 123025.

- [38] K. Yu, T. Ji, M. Wu, S. Chen, Y. Gao, J. Yan, S. Meng, W. Hu, X. Fan, W. Dong, J. Yin, Y. Liu, Supercritical ethane processing of ZIF-8 membranes towards pressure-resistant C₃H₆/C₃H₈ separation, Angew. Chem. Int. Ed. 64 (2025) e202422709.
- [39] L. Liu, W. Hu, Y. Sun, T. Ji, Y. He, K. Yu, M. Wu, G. He, Y. Liu, Coupling atomic layer deposition with supercritical fluid processing to provide a highly C₃H₆selective ZIF-8 membrane, AIChE J. 70 (2024) e18385.
- [40] L. Liu, M. Zhang, T. Ji, J. Yan, Y. Sun, G. He, Y. Liu, Sustainable fabrication of the zeolitic imidazolate Framework-67 membrane via supercritical fluid processing of the Co-Based gel layer, Chem. Mater. 33 (2021) 7350–7356.
- [41] Z. Zhang, E. Gou, Z. Zhao, R. Wu, R. Fang, W. Guo, J. Yao, Mixed matrix composite membranes comprising nanocage-like hollow ZIF-71(h) polyhedral nanocrystals in poly(ether-block-amide) membranes for phenol/water separation, Sep. Purif. Technol. 357 (2025) 130169.
- [42] A. Baniani, M.P. Rivera, R.P. Lively, S. Vasenkov, Quantifying diffusion of organic liquids in a MOF component of MOF/Polymer mixed-matrix membranes by high field NMR, J. Membr. Sci. 640 (2021) 119786.
- [43] F. Sahin, B. Topuz, H. Kalipcilar, ZIF filled PDMS mixed matrix membranes for separation of solvent vapors from nitrogen, J. Membr. Sci. 598 (2020) 117792.
- [44] H. Yin, C.Y. Lau, M. Rozowski, C. Howard, Y. Xu, T. Lai, M.E. Dose, R.P. Lively, M. L. Lind, Free-standing ZIF-71/PDMS nanocomposite membranes for the recovery of ethanol and 1-butanol from water through pervaporation, J. Membr. Sci. 529 (2017) 286–292.
- [45] Y. Li, L.H. Wee, J.A. Martens, I.F.J. Vankelecom, ZIF-71 as a potential filler to prepare pervaporation membranes for bio-alcohol recovery, J. Mater. Chem. A 2 (2014) 10034–10040
- [46] R. Banerjee, A. Phan, B. Wang, C. Knobler, H. Furukawa, M. O'Keeffe, O.M. Yaghi, High-throughput synthesis of zeolitic imidazolate frameworks and application to CO₂ capture, Science 319 (2008) 939–943.
- [47] K. Cui, S. Bhattacharyya, S. Nair, J.R. Schmidt, Origins of acid-gas stability behavior in zeolitic imidazolate frameworks: the unique high stability of ZIF-71, J. Am. Chem. Soc. 143 (2021) 18061–18072.
- [48] S. Calero, P. Gomez-Alvarez, Underlying adsorption mechanisms of water in hydrophobic and hydrophilic Zeolite Imidazolate frameworks: ZIF-71 and ZIF-90, J. Phys. Chem. C 119 (2015) 23774–23780.
- [49] X. Dong, Y.S. Lin, Synthesis of an organophilic ZIF-71 membrane for pervaporation solvent separation, Chem. Commun. 49 (2013) 1196–1198.
- [50] K. Huang, Q. Li, G. Liu, J. Shen, K. Guan, W. Jin, A ZIF-71 hollow fiber membrane fabricated by contra-diffusion, ACS Appl. Mater. Interfaces 7 (2015) 16157–16160.
- [51] S. Saha, S. Springer, M.E. Schweinefuss, D. Pontoni, M. Wiebcke, K. Huber, Insight into fast nucleation and growth of zeolitic imidazolate Framework-71 by in situ time-resolved light and X-ray scattering experiments, Cryst. Growth Des. 16 (2016) 2002–2010.
- [52] D. Li, M. Ye, C. Ma, N. Li, Z. Gu, Z. Qiao, Preparation of a self-supported zeolite glass composite membrane for CO₂/CH₄ separation, Smart Mol 2 (2024) e20240009.
- [53] I.C. Hou, L. Li, H. Zhang, P. Naumov, Smart molecular crystal switches, Smart Mol. 2 (2024) e20230031.
- [54] M. Tu, C. Wiktor, C. Roesler, R.A. Fischer, Rapid room temperature syntheses of zeolitic-imidazolate framework (ZIF) nanocrystals, Chem. Commun. 50 (2014) 13258–13260.
- [55] W. Bi, L. Han, Y. Liu, L. Li, The key to MOF membrane fabrication and application: the trade-off between crystallization and film formation, Chem. Eur J. 30 (2024) e202401868.
- [56] L. Liu, Y. Peng, K. Li, C. Zhu, W. Yang, Dual identity validation of a robust MOF membrane for efficient multiscenario CO₂ separation, Adv. Funct. Mater. (2024) 2404643.
- [57] Y. Wang, Q. Shi, H. Xu, J. Dong, The synthesis and tribological properties of small and large-sized crystals of zeolitic imidazolate framework-71, RSC Adv. 6 (2016) 18052–18059.
- [58] L. Liu, D. Zhang, Y. Zhu, Y. Han, Bulk and local structures of metal-organic frameworks unravelled by high-resolution electron microscopy, Commun. Chem. 3 (2020) 99
- [59] P. Banerjee, K.L. Kollmannsberger, R.A. Fischer, J.R. Jinschek, Mechanism of electron-beam-induced structural degradation in ZIF-8 and its electron dose tolerance, J. Phys. Chem. A 128 (2024) 10440–10451.
- [60] C. Wiktor, M. Meledina, S. Turner, O.I. Lebedev, R.A. Fischer, Transmission electron microscopy on metal—organic frameworks – a review, J. Mater. Chem. A 5 (2017) 14969–14989.
- [61] P. Su, H. Tang, M. Jia, Y. Lin, W. Li, Vapor linker exchange of partially amorphous metal-organic framework membranes for ultra-selective gas separation, AIChE J. 68 (2022) e17576.
- [62] M. Zhang, Q. Shang, Y. Wan, Q. Cheng, G. Liao, Z. Pan, Self-template synthesis of double-shell TiO₂@ZIF-8 hollow nanospheres via sonocrystallization with enhanced photocatalytic activities in hydrogen generation, Appl. Catal. B Environ. 241 (2019) 149–158.